*The AAPS Journal, Vol. 18, No. 3, May 2016 (© 2016)*
DOI: 10.1208/s12248-016-9887-0

*Research Article*

# Aggregation Kinetics for IgG1-Based Monoclonal Antibody Therapeutics

**A. Singla,[1] R. Bansal,[1] Varsha Joshi,[1] and Anurag S. Rathore[1,2]**

*Received 8 September 2015; accepted 11 February 2016; published online 22 February 2016*

***Abstract.*** Monoclonal antibodies (mAbs) as a class of therapeutic molecules are finding an increasing demand in the biotechnology industry for the treatment of diseases like cancer and multiple sclerosis. A key challenge associated to successful commercialization of mAbs is that from the various physical and chemical instabilities that are inherent to these molecules. Out of all probable instabilities, aggregation of mAbs has been a major problem that has been associated with a change in the protein structure and is a hurdle in various upstream and downstream processes. It can stimulate immune response causing protein misfolding having deleterious and harmful effects inside a cell. Also, the extra cost incurred to remove aggregated mAbs from the rest of the batch is huge. Size exclusion chromatography (SEC) is a major technique for characterizing aggregation in mAbs where change in the aggregates' size over time is estimated. The current project is an attempt to understand the rate and mechanism of formation of higher order oligomers when subjected to different environmental conditions such as buffer type, temperature, pH, and salt concentration. The results will be useful in avoiding the product exposure to conditions that can induce aggregation during upstream, downstream, and storage process. Extended Lumry-Eyring model (ELE), Lumry-Eyring Native Polymerization model (LENP), and Finke-Watzky model (F-W) have been employed in this work to fit the aggregation experimental data and results are compared to find the best fit model for mAb aggregation to connect the theoretical dots with the reality.

**KEY WORDS:** Aggregation; Monoclonal antibody; Lumry-Eyring Nucleated Polymerization model; Finke-Watzky model; Extended Lumry-Eyring model.

## INTRODUCTION

Monoclonal antibodies (mAbs) have emerged as the moieties of choice for treatment of various diseases ranging from chronic diseases like rheumatoid arthritis, psoriasis, asthma to fatal diseases like cancer, multiple sclerosis, and ebola (1–4). However, product instability continues to be a concern among manufacturers of protein therapeutics, particularly in the form of protein aggregation which may result in the loss of biological activity as well as toxicity (5–8). While these effects are likely to vary from mAb to mAb, the need to minimize aggregation is universally recognized (4).

Aggregation can take place during protein expression in cell culture, purification in downstream processing, formulation, and/or storage (4,6). Protein molecules can aggregate *via* physical association (primary structure unchanged) or by chemical bond formation. Either of them may induce soluble or insoluble aggregates. Over the past few decades, several researchers have proposed different mechanisms of aggregation including (i) reversible association of the native monomer, (ii) aggregation of conformationally altered monomer, (iii) aggregation of chemically modified product, (iv) nucleation-controlled aggregation, and (v) surface induced aggregation (9–12).

Factors that are known to significantly affect protein aggregation can be broadly classified as internal and external factors. Internal factors relate to changes in the primary and secondary structure of the protein. Tendency of a protein to aggregate is generally considered as a function of its sequence. Changes in the protein sequence either by mutation or chemical alteration can alter its hydrophobicity as well as surface charge distribution and hence, the tendency to aggregate. Internal factors also include changes in the secondary structure of the protein (alpha and beta content). On the contrary, external factors include different environmental factors that may affect the aggregation propensity of a protein. These include pH, temperature, salt concentration, buffer type, protein concentration, ionic strength, mixing, shear, metal ions, pressure, freeze-thawing, freeze-drying, and reconstitution (6,12).

Kinetic studies and modeling of the resulting data have been shown to be useful for understanding the underlying mechanisms behind aggregation (13). When combined with experimental kinetic and thermodynamic data, mathematical models of aggregation kinetics can provide a non-invasive way to gain qualitative and quantitative insights into the aggregation mechanism (14). This in turn can help in designing precise experiments to more accurately predict and control aggregation rates by choosing appropriate conditions and hold times. Of the various mathematical

[1] Department of Chemical Engineering, Indian Institute of Technology, Hauz Khas, New Delhi, 110016, India.
[2] To whom correspondence should be addressed. (e-mail: asrathore@biotechcmz.com), URL: http://www.biotechcmz.com

models that have been proposed to predict the kinetics of protein aggregation, the Lumry-Eyring model has been commonly used (15–18). This model identifies aggregation as a simple, two-step, non-native mechanism: rate limiting reversible conformational transitions of the protein followed by irreversible conglomeration of proteins into aggregates (15,16). Later, the Extended Lumry-Eyring (ELE) model has been proposed to further distinguish between the different kinds of aggregated molecules based on the number of monomer chains that constitute them (19). Compared to the classical model, this model describes the intrinsic kinetics of aggregation in detail. This model has been further adapted to account for nucleated polymerization in the form of the Extended Lumry-Eyring with Nucleated Polymerization (LENP) model (14,20). Other than these, the Finke-Watzky model has also been recently applied to a broad spectrum of aggregating proteins like amyloid β, prions, etc. (21,22). In addition to this, some aggregate condensation and polymerization models which account for very higher order aggregate condensation into even larger aggregates and hence have not been used in this study (14,20).

In a previously published study, we have elucidated the importance of establishing hold times during mAbs processing (6,23). In this paper, we focus on evaluation of the aggregation kinetics for immunoglobulin (IgG1)-based mAb therapeutics. Effects of various external factors such as pH, temperature, buffer species, and salt concentration on mAb aggregation have been investigated. Utilities of Finke-Watzky (F-W), ELE and LENP models have been explored to achieve the above-mentioned objective.

## MATERIALS AND METHODS

### Feed Materials

An IgG1 antibody (procured from Biocon Limited, Bengaluru, Karnataka, India) with a pI of 8.5 was used in this study. The mAb was stored at 4°C, pH 7.0, at a concentration of 30 mg/ml in a buffer containing 15 mM sodium phosphate, 150 mM NaCl, and 0.1% sodium azide. The latter was used to avoid bacterial contamination during storage.

### Reagents

Table I lists all the buffers that were examined in this study. These are the buffers which are commonly employed during downstream processing of mAbs for Protein A chromatography (acetate, glycine, and citrate at pH 3.0 with 0–100 mM NaCl), cation exchange chromatography (phosphate, citrate, and acetate at pH 6.0–7.5 with 0–200 mM NaCl), and anion exchange chromatography (tris and phosphate at pH 7.2–8.0). All buffers were filtered using a 0.22-μm cutoff nylon membrane filter (PALL Life Sciences, Port Washington, NY, USA) and then degassed. All chemicals were procured from Merck, India. All reagents used for size exclusion chromatography (SEC) were of HPLC grade (Sigma Aldrich, Bengaluru, Karnataka, India).

### Sample Preparation

The required buffer composition, as per Table I, was achieved by performing gel filtration chromatography-based buffer exchange using a Sephadex G-25 resin (GE Healthcare Biosciences, Pittsburgh, PA, USA) packed into a Tricon™ column (100 × 10 mm). After buffer exchange, three temperature conditions (4, 15, and 30°C) were used to store the 3.5-ml aliquots. Aggregation studies were performed for 0–120 h at intermittent time points.

Concentration of the protein in the samples was measured by UV–VIS spectroscopy at 280 nm using a Spectra Max M2e Multimode Microplate Reader (Molecular Devices, Sunnyvale, CA, USA) in congruence to the Lambert-Beer Law. Sample readings were recorded in duplicate and normalized by subtracting the readings from the blank buffer. A dilution factor of 10 and extinction coefficient of 1.41 has been used for the estimation purposes. In each case, the sample concentration was measured after buffer exchange and the final concentration was adjusted to 10 mg/ml with the respective buffer.

### Size Exclusion Chromatography

SEC was performed with a Superdex™ 200, 10 mm × 300 mm high resolution column (GE Healthcare Biosciences, Pittsburgh, PA, USA) operated at 25°C. The column was mounted on a Thermoscientific Dionex Ultimate 3000 HPLC unit (Thermo Scientific, Sunnyvale, CA, USA) consisting of a quaternary pump with a degasser, an auto sampler with a cooling unit, and a variable wavelength detector (VWD). Isocratic elution was performed for 45 min at a flow rate of 0.5 ml/min with 50 mM phosphate buffer, 300 mM NaCl, and 0.05% $NaN_3$ at pH 7.0. All buffers were filtered with a 0.22-μm cutoff nylon membrane filter (PALL Life Sciences, Port Washington, NY, USA) and degassed prior to use. The monomer peaks were characteristically distinct but peaks for other species were overlapped with each other. Chromeleon software (Thermo Scientific, Sunnyvale, CA, USA) was used for estimating the residual monomer concentration by computing the percentage area under the monomer peak in the non-normalized SEC chromatograms. Detection was performed by monitoring UV absorbance at 280 nm.

### Dynamic Light Scattering (DLS)

The hydrodynamic radii of the solutions obtained from SEC, corresponding to different types of mAb monomer association, were determined using a Zetasizer Nano ZS 90 (Malvern Instruments, UK) particle size analyzer with temperature control fitted with a 633-nm He-Ne laser. The instrument uses dynamic light scattering to measure the diffusion coefficient, $D$, which is then converted to an average hydrodynamic size $R_H$ of mAbs in solution using the Stokes-Einstein equation (24):

$$R_{\mathrm{H}} = \frac{k_{\mathrm{B}}T}{6\pi\eta_{\mathrm{s}}D} \tag{1}$$

where $k_B$ is the Boltzmann constant, $T$ is absolute temperature (25°C for all experiments carried out in the current study), and $\eta_s$ is the solvent viscosity (for the

**Table I.** Buffer Conditions Examined in this Experimental Study (23). Product Concentration Was 10 mg/ml mAb in All Cases

| Type of process chromatography | Buffers examined | pH | Salt concentration | Temperature |
|---|---|---|---|---|
| Protein A chromatography | 100 mM citrate | 3.0 | 0 mM NaCl | 4°C |
| | | | | 15°C |
| | | | | 30°C |
| | | | 50 mM NaCl | 4°C |
| | | | | 15°C |
| | | | | 30°C |
| | | | 100 mM NaCl | 4°C |
| | | | | 15°C |
| | | | | 30°C |
| | 100 mM acetate | 3.0 | 0 mM NaCl | 4°C |
| | | | | 15°C |
| | | | | 30°C |
| | | | 100 mM NaCl | 4°C |
| | | | | 15°C |
| | | | | 30°C |
| | 100 mM glycine | 3.0 | 0 mM NaCl | 4°C |
| | | | | 15°C |
| | | | | 30°C |
| | | | 100 mM NaCl | 4°C |
| | | | | 15°C |
| | | | | 30°C |
| Anion exchange chromatography | 20 mM Tris HCl | 7.2 | 50 mM NaCl | 4°C |
| | | | | 30°C |
| | | 8.0 | 0 mM NaCl | 4°C |
| | | | | 30°C |
| Cation exchange chromatography | 20 mM citrate | 6.0 | 0 mM NaCl | 4°C |
| | | | | 30°C |
| | | | 200 mM NaCl | 4°C |
| | | | | 30°C |
| | 25 mM acetate | 6.0 | 0 mM NaCl | 4°C |
| | | | | 30°C |
| | | | 200 mM NaCl | 4°C |
| | | | | 30°C |
| | 15 mM phosphate | 6.5 | 0 mM NaCl | 4°C |
| | | | | 30°C |
| | | | 200 mM NaCl | 4°C |
| | | | | 30°C |
| | | 7.5 | 0 mM NaCl | 4°C |
| | | | | 30°C |
| | | | 200 mM NaCl | 4°C |
| | | | | 30°C |

current study, a measured value of $\eta_s$ has been taken to be 0.8 mPa.s). The scattered intensities from mAb solutions were recorded at a fixed scattering angle of 90° (this greatly reduces the effects of dust in the solution). An extensive sample preparation method was followed to ensure repeatability. The cuvette was washed with ethanol for five times and kept for 15 min inside laminar air flow. It was followed by wash with milliQ grade water for 10 to 15 min continuously. In the meantime, the mAb solutions were filtered with 0.4 μm membrane filter (Pall Corp., USA) with at least two different membranes consecutively. The dilution of the sample solutions was checked by recording UV absorbance at 280 nm. The instrument has the ability to measure a wide size range (0.3 to 5000 nm in diameter) and the diameters that are reported in this study ranges from 10 to 210 nm, which is within the size range of the instrument.

### Determination of Oligomer Types

Molecular mass of various oligomers that were formed during the study was determined by using a standard gel filtration marker kit (Sigma Aldrich, St. Louis, MO, USA). The seven protein markers of known molecular weights (29–2000 kDa) were run through the same system used for SEC and the elution times were noted. Since molecular size is directly related to the molecular weight, the protein with the least molecular weight, Carbonic Anhydrase Bovine Erythrocytes (molecular weight 29 kDa), elutes at the end, while Blue Dextran with the highest molecular weight of 2000 kDa elutes at the beginning (Fig. 1a). A semi-logarithmic calibration curve of molecular mass *versus* $V_e/V_o$ was plotted for these proteins (Fig. 1b), where $V_e$ is the elution volume for each protein and $V_o$ is the pore

volume of the column. Using this calibrated curve, the molecular mass for different oligomers eluting at different times was determined for the samples being used in this study (Fig. 1c). A ratio of this molecular weight to the monomer molecular weight denotes the number of monomer units present in each oligomer. If the number of monomer units in an oligomer was observed to be between x and x.5, then the oligomer was assumed to contain x monomer units and if these units lied between x.5 and x+1, then the oligomer was assumed to contain x+1 monomer units.

The oligomer distribution was also confirmed using DLS. First, DLS was performed on the seven proteins from the standard gel filtration markers kit and the hydrodynamic diameter corresponding to each protein was noted. Next, a correlation between hydrodynamic diameter and molecular weight was determined (Fig. 1d). Oligomers corresponding to the different peaks as observed in the SEC chromatograms were pooled separately and DLS was performed on each fraction. The hydrodynamic diameter for these separate peaks was fit into the correlation obtained above to determine the molecular weights of these separate peaks. The oligomer distribution obtained using DLS (Fig. 1) was in agreement with the SEC results and it is seen that some samples have monomer, dimer, trimer, tetramer, and pentamer species.

## Circular Dichroism (CD)

Changes in the secondary structure of the protein were monitored by performing Far-UV CD analysis on a Jasco J-815 CD spectrometer (Mary's Court, Easton, MD, USA). Sample concentration was kept at 0.2 mg/ml and wavelength in the range of 200–250 nm was used to obtain spectra (25). For spectral measurements, quartz cuvette (1 mm path length) was used at 20°C and an average of five scans was taken. CD spectra of the buffer solution were subtracted from the sample spectra before conversion to absolute CD values. The mean residual ellipticity values (MRE) at wavelength $\lambda$ ($[\theta]_{MRW,\ \lambda}$) were calculated using the mean residual weight (MRW) for the antibody as follows (25):

$$[\theta]_{MRW,\lambda} = \frac{(MRW)\theta_\lambda}{10\,d\,c} \tag{2}$$

where $\theta_\lambda$ is the observed ellipticity (degrees) at wavelength $\lambda$, $d$ is the path length (cm), and $c$ is the concentration (g/ml).

## Data Analysis and Kinetic Modeling

Data was analyzed and kinetic modeling was done using MATLAB R2011a for ELE and LENP models. The

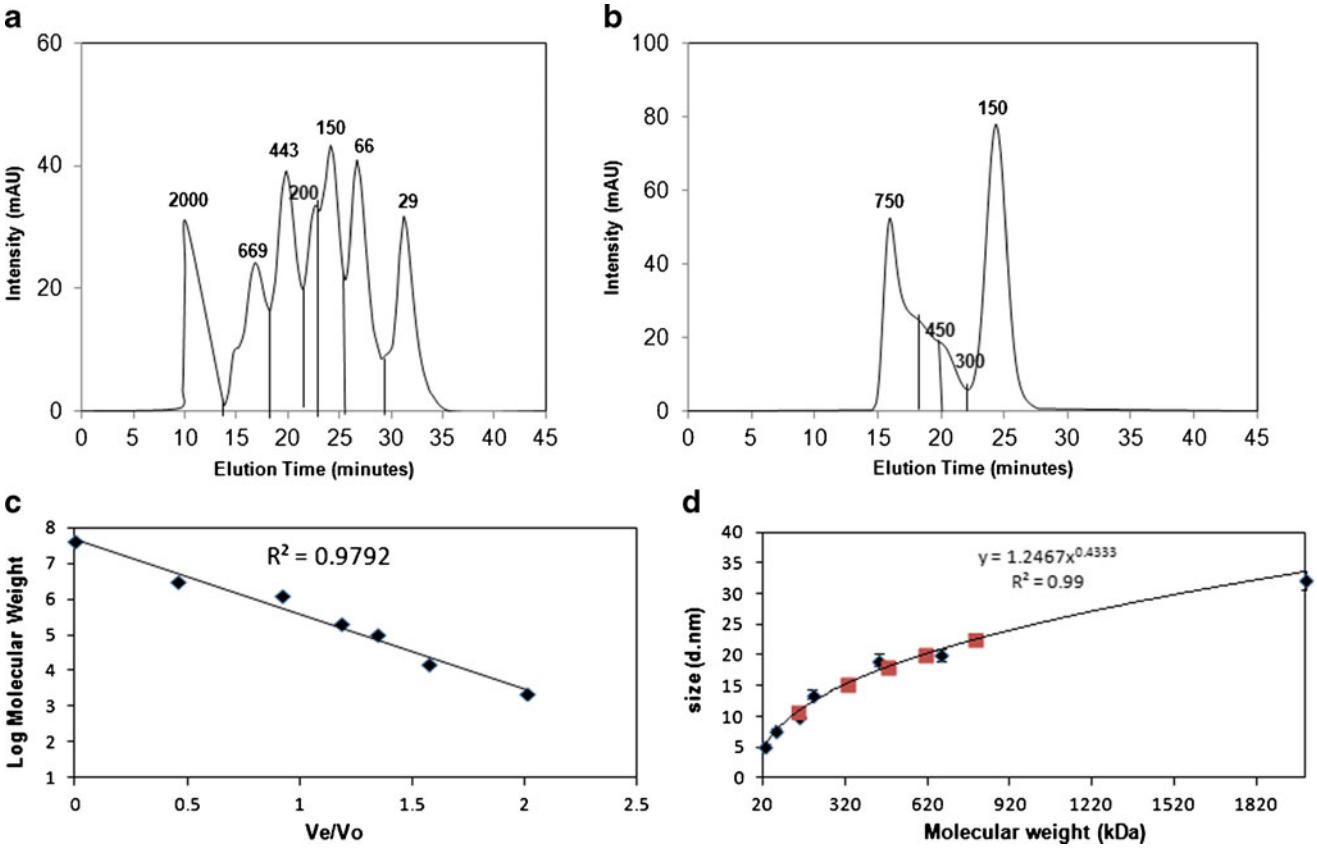


**Fig. 1.** SEC chromatograms and DLS data for oligomer distribution analysis. **a** Elution times of the seven proteins in the gel filtration marker kit as determined by SEC; **b** Elution times of different oligomers observed at the 75th hour for 10 mg/ml mAb in 100 mM acetate, 100 mM NaCl, pH 3.0 and 30°C as determined by SEC. **c** Semi-logarithmic calibration curve of molecular weight *v/s* normalized elution volume used for oligomer distribution analysis. **d** Hydrodynamic diameter obtained from DLS *v/s* molecular weights of proteins, (*black diamond*) seven proteins from gel filtration markers kit, (*red square*) oligomers corresponding to different peaks in SEC chromatograms

mathematical equations involved a set of ordinary differential equations (ODEs) which needed to be solved simultaneously. Gauss-Newton algorithm was employed to fit the experimental data to these differential equations and model parameters were estimated (26).

## THEORY

### Finke-Watzky model

"Ockham's razor"/minimalistic F-W model assumes slow nucleation followed by fast autocatalytic growth. The two steps are characterized by the respective average rate constants for nucleation ($k_1$) and growth ($k_2$) (21). If $A$ represents a precatalytic form of the protein monomer and $B$ represents a catalytic aggregated form of the protein past the critical nucleus size, the model can be expressed as (13):

$$A \xrightarrow{k_1} B \tag{3}$$

$$A + B \xrightarrow{k_2} 2B \tag{4}$$

$$[A]_t = \frac{\frac{k_1}{k_2} + [A]_o}{1 + \frac{k_1}{k_2[A]_o} e^{(k_1 + k_2[A]_o)t}} \tag{5}$$

$$[B]_t = [A]_o - \frac{\frac{k_1}{k_2} + [A]_o}{1 + \frac{k_1}{k_2[A]_o} e^{(k_1 + k_2[A]_o)t}} \tag{6}$$

Where $[A]_t$ and $[B]_t$ are molar concentrations of $A$ and $B$, respectively, at any time $t$ and $[A]_0$ is the initial molar concentration of $A$. In this model, all aggregate species irrespective of the association type (dimers, trimers, etc.) are considered kinetically equivalent species and all are accounted for together in $B$. Within the F-W model, the actual steps occurring at the molecular level of the aggregation process can be combined into two pseudoelementary steps as shown in Eqs. 3 and 4. The F-W model assumes that the rate of growth is significantly more than the rate of nucleation, i.e., $k_2 >> k_1$.

### Extended Lumry-Eyring model

The ELE model accounts for the reversible conformational changes as well as the conformationally mediated irreversible aggregation (19). The unfolding and refolding of native monomer state ($N$) to different unfolded states is accounted for as a single reversible equation and all the reactive monomer states prone to aggregation are represented together as $R_A$. With respect to the aggregation process, species $N$ and $R_A$ are assumed to reach thermodynamic equilibrium instantaneously with equilibrium constant ($K_{NR}$). For the ELE model, protein unfolding is the rate determining step and the aggregation reaction is of second order. In our study, we did not observe any precipitation and hence our focus was primarily on the formation of soluble aggregates.

The reaction scheme for ELE model (19) is as follows:

$$N \overset{K_{\mathrm{NR}}}{\longleftrightarrow} R_{\mathrm{A}} \tag{7}$$

$$R_{\mathrm{A}} + R_{\mathrm{A}} \overset{K_{1,1}}{\rightarrow} A^{(2)} \tag{8}$$

$$A^{(2)} + R_{\mathrm{A}} \overset{K_{1,2}}{\rightarrow} A^{(3)} \tag{9}$$

$$A^{(3)} + R_{\mathrm{A}} \overset{K_{1,3}}{\rightarrow} A^{(4)} \tag{10}$$

$$\vdots$$

$$A^{(n^*-1)} + R_{\mathrm{A}} \overset{K_{1,n^*-1}}{\rightarrow} A^{(n^*)} \tag{11}$$

$$A^{(2)} + A^{(2)} \overset{K_{2,2}}{\rightarrow} A^{(4)} \tag{12}$$

$$A^{(2)} + A^{(3)} \overset{K_{2,3}}{\rightarrow} A^{(5)} \tag{13}$$

$$\vdots$$

$$A^{(i)} + A^{(j)} \overset{K_{i,j}}{\rightarrow} A^{(i+j)} \qquad i, j < n^* \tag{14}$$

The various terms used in the above reaction schemes are defined as follows: $N$ is the native state (monomer), $R_{\mathrm{A}}$ is the monomer in aggregation prone state, $K_{ij}$ is the intrinsic rate constant for aggregation of an $i$-mer with a $j$-mer, and $n^*$

is the size cutoff for protein aggregates having appreciable solubility with respect to aggregation.

This model can be summarized through mathematical equations as:

$$\frac{dN}{dt} = -k_{\mathrm{u}}\left(N - K_{\mathrm{NR}}^{-1} R_{\mathrm{A}}\right) \tag{15}$$

$$\frac{dR_{\mathrm{A}}}{dt} = k_{\mathrm{u}}\left(N - K_{\mathrm{NR}}^{-1} R_{\mathrm{A}}\right) - 2k_{1,1}R_{\mathrm{A}}^2 - \left(\sum_{j=2}^{n^*-1} k_{1,j}A_j\right) R_{\mathrm{A}} \tag{16}$$

$$\left.\frac{dA_j}{dt}\right|_{2 \le j \le n^*} = \left(\sum_{\substack{v<w \\ v+w=j}} k_{vw}A_vA_w\right) - \left(\sum_{i=2}^{n^*-1} k_{ij}A_iA_j\right) - k_{jj}A_j^2 - k_{1j}A_jR_{\mathrm{A}} \tag{17}$$

where $K_{NR} = k_u/k_f$, $k_u$ is the forward reaction rate constant for unfolding of $N$ to $R_A$, $k_f$ is the reaction rate constant for refolding of $R_A$ back to $N$, $n^*$ is the highest order of soluble aggregate observed, and $A_x$ is the aggregate containing $x$ monomer units. Thus, $A_1$ is equivalent to $R_A$. Further, $k_{ij}$ is the reaction rate constant for the irreversible reaction between $A_i$ and $A_j$. Since the monomer cannot be distinguished into $N$ and $R_A$ experimentally, $N$ and $R_A$ are considered together as monomer ($M$) for calculations.

$$M = N + R_{\mathrm{A}} \tag{18}$$

$$f_{\mathrm{R}} \equiv \frac{K_{\mathrm{NR}}}{1 + K_{\mathrm{NR}}} \tag{19}$$

where $f_R$ is the fraction of $M$ existing as $R_A$. Equations 15 to 17 can then be expressed as:

$$\frac{dM}{dt} = -2k_{11}f_{\mathrm{R}}^2M^2 - f_{\mathrm{R}}\left(\sum_{j=2}^{n^*-1} k_{1j}A_j\right)M \tag{20}$$

$$\left.\frac{dA_j}{dt}\right|_{2 \le j \le n^*} = \left(\sum_{\substack{v<w \\ v+w=j}} k_{vw}A_vA_w\right) - \left(\sum_{i=2}^{n^*-1} k_{ij}A_i\right)A_j - k_{jj}A_j^2 - k_{1j}f_{\mathrm{R}}A_jM \tag{21}$$

For simplicity, $k_{11}{f_R}^2$ and $k_{1j}f_R$ are taken as $k_{11,app}$ and $k_{1j,app}$, respectively (i.e., apparent rate constants). These apparent rate constants contain two aspects: (a) conformational stability behavior of mAb represented by $f_R$ and (b) kinetic colloidal stability of solution represented by $k_{ij}$ (17). These aspects are interrelated to each other and their individual effect on aggregation cannot be distinguished. Symbols $N$, $R_A$, $M$, and $A_x$ in the equations (15–21) represent molar concentrations at any time $t$. Concentration data obtained from the experiments is then fitted into these equations *via* the Gauss-Newton method using MATLAB R2011a to estimate these apparent rate constants at each step (26). These have been used as parameters to fit the experimental data into the model.

### Lumry-Eyring Nucleated Polymerization

The LENP model is a more generalized model and incorporates the concept of nucleation into the aggregation process (14). The model assumes that kinetic regimes distinguished experimentally by a combination of (i) apparent reaction order, (ii) dependence on the initial protein concentration, and (iii) aggregate size distribution (13). The reaction schemes for LENP model (14) can be stated as follows:

I. Conformational transitions of folding-component monomers

$$N \overset{K_{NI}}{\longleftrightarrow} I \overset{K_{IU}}{\longleftrightarrow} U \tag{22}$$

II. Reversible associations of $R$ monomers (pre-nucleation)

$$2R \overset{K_2}{\longleftrightarrow} R_2 \tag{23}$$

$$\vdots$$

$$(x-1)R \overset{K_{x-1}}{\longleftrightarrow} R_{x-1} \tag{24}$$

III. Nucleation including rearrangement from $R_x$ to $A_x$

$$R + R_{x-1} \underset{K_{\mathrm{d},x}}{\overset{K_{\mathrm{a},x}}{\leftrightarrow}} R_x \overset{K_{r,x}}{\rightarrow} A_x \tag{25}$$

IV. Growth of soluble, higher-MW aggregates via monomer addition

$$A_j + R \overset{K_{\mathrm{RA}}}{\longleftrightarrow} \left(A_jR\right) \tag{26}$$

$$\vdots$$

$$A_jR_{\delta-1} + R \underset{k_{\mathrm{d}}}{\overset{K_{\mathrm{a}}}{\leftrightarrow}} \left(A_jR_\delta\right) \overset{K_r}{\rightarrow} A_{j+\delta} \quad x \le j < n^* \tag{27}$$

V. Condensation: aggregate-aggregate assembly

$$A_i + A_j \overset{K_{i,j}}{\rightarrow} \cdots \rightarrow \text{Fibrils, precipitates, gels} \quad i, j \ge n^* \tag{28}$$

where, $N$ is the native state (monomer), $I$ is the intermediate state (monomer), $U$ is the unfolded state, $R$ is the reactive monomer, $x$ is the nucleus size, $A_x$ is the aggregate nucleus, $A_j$ is the aggregate composed of $j$ monomers, $R_x$ is the reversible

aggregate prenucleus, $A_jR$ is the reversibly associated $A_j$ and $R$, $K_{NI}$ is the equilibrium constant for $N \leftrightarrow I$, $K_{IU}$ is the equilibrium constant for $I \leftrightarrow U$, $K_a$ is the association rate coefficient, $K_d$ is the dissociation rate coefficient, $K_{a,x}$ is $K_a$ for nucleation step, and finally $K_{d,x}$ is $K_d$ for the nucleation step.

A number of parameters have been considered in this model, namely the nucleus stoichiometry ($x$), monomers added in each growth step ($\delta$), and the inverse rate coefficients for nucleation and growth which also signify their corresponding time scales ($\tau_n$ and $\tau_g$) (27). Equations 22–28 can be expressed in the form of the following differential equations:

$$\frac{dm}{dt} = -\frac{xm^x}{\tau_n} - \frac{\delta m^\delta \sum_i a_i}{\tau_g} \tag{29}$$

$$\frac{da_x}{dt} = \frac{m^x}{\tau_n} - \frac{m^\delta a_x}{\tau_g} \tag{30}$$

$$\frac{da_i}{dt} = \frac{m^\delta}{\tau_g}(a_{i-\delta} - a_i) \tag{31}$$

$$\frac{da_{n^*}}{dt} = \frac{m^\delta}{\tau_g}(a_{n^*-\delta}) \tag{32}$$

where $m = [M]/[M]_o, a_i = [A_i]/[M]_o$and $x < i < n^*[M]$ and $[A_i]$ are molar concentrations of monomer and aggregate (containing "$i$" monomer units), respectively, at any time $t$. $[M]_o$ is the initial molar concentration of monomer and $n^*$ represent the order of highest oligomer observed in the solution. The limiting step for LENP is the rearrangement step (step III).

## RESULTS

Aggregate levels were monitored *via* SEC and CD spectroscopy at various conditions presented in Table I. Effects of different factors (pH, salt concentration, buffer, and temperature) on aggregation were analyzed. Table II presents a summary of the aggregation behavior that was seen under various storage conditions. It was seen that aggregation is high at low pH and worsens with addition of salt and increase in temperature (23). Aggregation was minimal under most conditions at high pH. These reactions are considered irreversible and this has been confirmed by performing the experiments where these aggregate species were found to be irreversible and there is no change in aggregate content after dilution of these aggregate samples (2×, 4×, 8×, 16×) and incubating them for 6 h.

### Identification of Oligomers by DLS

As described above, DLS was used to obtain a size distribution as a plot of the relative intensity of light scattered by particles in various size classes as a function of hydrodynamic size (diameter) (Fig. 2a). It is evident from the data that the first peak (with the smallest diameter) corresponds to the mAb monomer and has a diameter of around 12 nm. This is in agreement with the values that have been reported in published studies (17). The authenticity of the data was ascertained from the observations that the diffusivity constants corresponding to the SEC elutes as obtained through DLS were of the same order of magnitude for all the species and that a steady decrease in the mean particle count rate was observed as the proportion of aggregation increases in the sample. As expected, a shift is observed in the maximum peak in the size distribution by intensity towards bigger sizes as aggregation proceeds. It is well known that the resulting structure for trimer and onwards deviates from a truly spherical shape (28) and that the scattering intensity has a non-linear (power-law) dependence on the molecular size (29). This is what we also observe in Fig. 2b and a power-law dependence is seen between the molecular sizes of monomer and aggregate species and the number of monomer units. Using the data corresponding to the mononer, dimer, and trimer could be extrapolated to identify the specie eluting as the first peak in the SEC chromatogram as pentamer.

### Effect of pH

Low pH (3.0–4.0) is commonly used for elution *via* protein A chromatography and for viral inactivation (30). It is, however, known to accelerate aggregation by causing significant changes in the *Fc* domain of an antibody (17,30). Figure 3a illustrates aggregation behavior of the product in citrate buffer at 30°C at pH 3.0 and 6.0. It is evident that aggregation is quite significant at pH 3.0 and minimal at pH 6.0. An overview of the data presented in Table II also supports the conclusion that aggregation primarily occurs at low pH (3.0) and is minimal at high pH values (6.0, 6.5, 7.2, 7.8, and 8.0).

Analysis of samples by CD spectroscopy was also performed and the results are shown in Fig. 4. It is observed that at low pH, the MRE values become positive as the time progresses and this signifies that there are structural changes in the protein molecule which lead to conformational loss and subsequently aggregate formation (Fig. 4a) (23). It should be noted that there are differences observed in the final % aggregate in comparison to what has been previously observed and reported (23). The reason for this is that though the starting material in the two cases was from the same product but it came from different batches and had different % aggregate at time $t = 0$. As a result, while the trends observed are identical, the actual values are not.

### Effect of Temperature

The rate of aggregation is expected to increase with temperature (8,12). Figure 3b illustrates the change in aggregation when temperature is increased from 4° C to 30°C. The conditions used were acetate, pH 3.0, 100 mM NaCl, and 30°C. The dramatic increase in the aggregation rate with

**Table II.** Percentage of Aggregate Content After 120 h of Incubation in a Variety of Storage Conditions. Salt Concentrations Used Are: (a) Citrate, pH 3.0, 100 mM NaCl, (b) Citrate, pH 6.0, 200 mM NaCl, (c) Acetate, pH 3.0, 100 mM NaCl, (d) Acetate, pH 6.0, 200 mM NaCl, (e) Glycine, pH 3.0, 100 mM NaCl, (f) Phosphate, pH 6.5 and 7.5, 200 mM NaCl; (g) Tris HCl, pH 7.2, 50 mM NaCl. Colors Represent the Level of Variation: \raster(100%,p)=":1::\\pdgts1174\springer\jwf\figures\TAJ\TAJ69887\s12248-016-9887-0Fmca.eps" Minimal Variation, \raster(100%,p)=":1::\\pdgts1174\springer\jwf\figures\TAJ\TAJ69887\s12248-016-9887-0Fmcb.eps" Moderate Variation, \raster(100%,p)=":1::\\pdgts1174\springer\jwf\figures\TAJ\TAJ69887\s12248-016-9887-0Fmcc.eps" High Variation, and ND—Not Determined. Product Concentration Was 10 mg/ml in All Cases

| Buffers | pH | Temperature 4 °C | | Temperature 30 °C | |
|---|---|---|---|---|---|
| | | Without NaCl | With NaCl | Without NaCl | With NaCl |
| Citrate | 3.0 | 8.35 | 15.48 | 83.53 | 91.59 |
| | 6.0 | 4.23 | 4.13 | 4.89 | 4.84 |
| Acetate | 3.0 | 4.77 | 16.01 | 4.31 | 79.11 |
| | 6.0 | 5.18 | 5.14 | 5.06 | 5.08 |
| Glycine | 3.0 | 4.02 | 6.82 | 3.97 | 40.8 |
| Phosphate | 6.5 | 4.27 | 4.36 | 3.62 | 4.51 |
| | 7.5 | 4.54 | 4.52 | 4.48 | 4.60 |
| Tris HCl | 7.2 | ND | 4.82 | ND | 4.95 |
| | 8.0 | 4.82 | ND | 4.27 | ND |

temperature has been observed in other cases too (Table II). Though we do not have conclusive evidence to confirm this, a possible reason for this increase could be a partial or complete unfolding of mAb at high temperatures, resulting in destabilization and formation of non-covalent aggregates as has been reported by numerous researchers (4,31–39).

Figure 4b illustrates the changes in CD spectra at 4° C and 30°C, respectively. At higher temperature, as the time progresses, the MRE values are continuously decreasing and this signifies that there is a conformational change in the protein. This also correlates with higher order aggregation observed at higher temperatures (25).

### Effect of Salt Concentration

Presence of salt is likely to induce aggregation of mAb products (40). However, the significance of this effect depends on salt type, salt concentration, interaction between protein and salt, and on the net charge of protein. The effect could either be an enhancement or deterioration of protein stability (40). Figure 3c illustrates the effect of presence of salt on mAb aggregation. The conditions used were acetate, 30°C and pH 3.0. It is seen that the rate of aggregation increases in the presence of salt.

These results are also consistent with the changes in CD spectra (Fig. 4c). There was a decrease observed in the MRE values at 218 nm in 100 mM NaCl compared to 0 mM NaCl. This indicates a conformational change in protein structure, a likely cause of aggregation (4,31–39).

### Effect of Buffer Species

It is seen in Fig. 3d that the aggregation behavior is different for the three buffers examined at pH 3.0 (citrate, acetate, glycine). The conditions used were 100 mM NaCl and 30°C in all cases. Citrate is found to be the only buffer which induces aggregation even in the absence of salt.

The results obtained from CD spectroscopy are also in agreement with those from SEC. The reduction in MRE values at 218 nm is more for acetate buffer than glycine buffer (Fig. 4d), indicating that of the three buffers examined, glycine buffer offers maximum product stability at pH 3.0. As soon as the mAb is exposed to the citrate buffer at pH 3.0, a significant shift in minima towards 230 nm (data not shown here) is observed indicating a substantial change in the secondary structure, likely resulting in enhanced aggregation (Fig. 4d). One of the possible explanations for this can be the rearrangement of aromatic amino acids (tryptophan and tyrosine) in the citrate buffer (both in presence and absence of salt) environment (23). This behavior is consistent with the effect of buffer species on stability of mAb therapeutics that have been reported in the literature (23).

The results presented in Table II and Figs. 3 and 4 indicate that pH plays the most significant role in protein

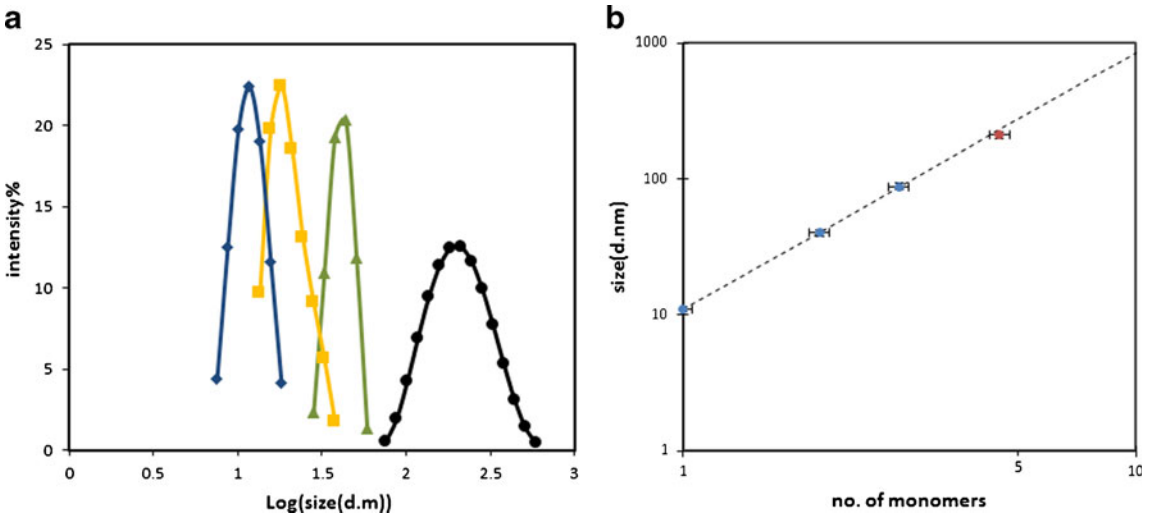


**Fig. 2.** DLS data of various aggregate species separated by SEC. **a** Semilogarithmic curve showing variation in intensity percent against diameter size of different aggregate species, (*pale blue circle*) monomer, (*yellow square*) dimer,(*pale green triangle*) trimer, (*black circle*) pentamer. **b** Curve representing size of various aggregate species *v/s* number of monomer units present in aggregate species on a logarithmic scale, (*pale blue circle*) monomer, dimer, trimer (from DLS measurement), (*red circle*) Pentamer (from curve extrapolation). All experiments were performed in triplicate and the *error bars* show the difference between raw data and the average

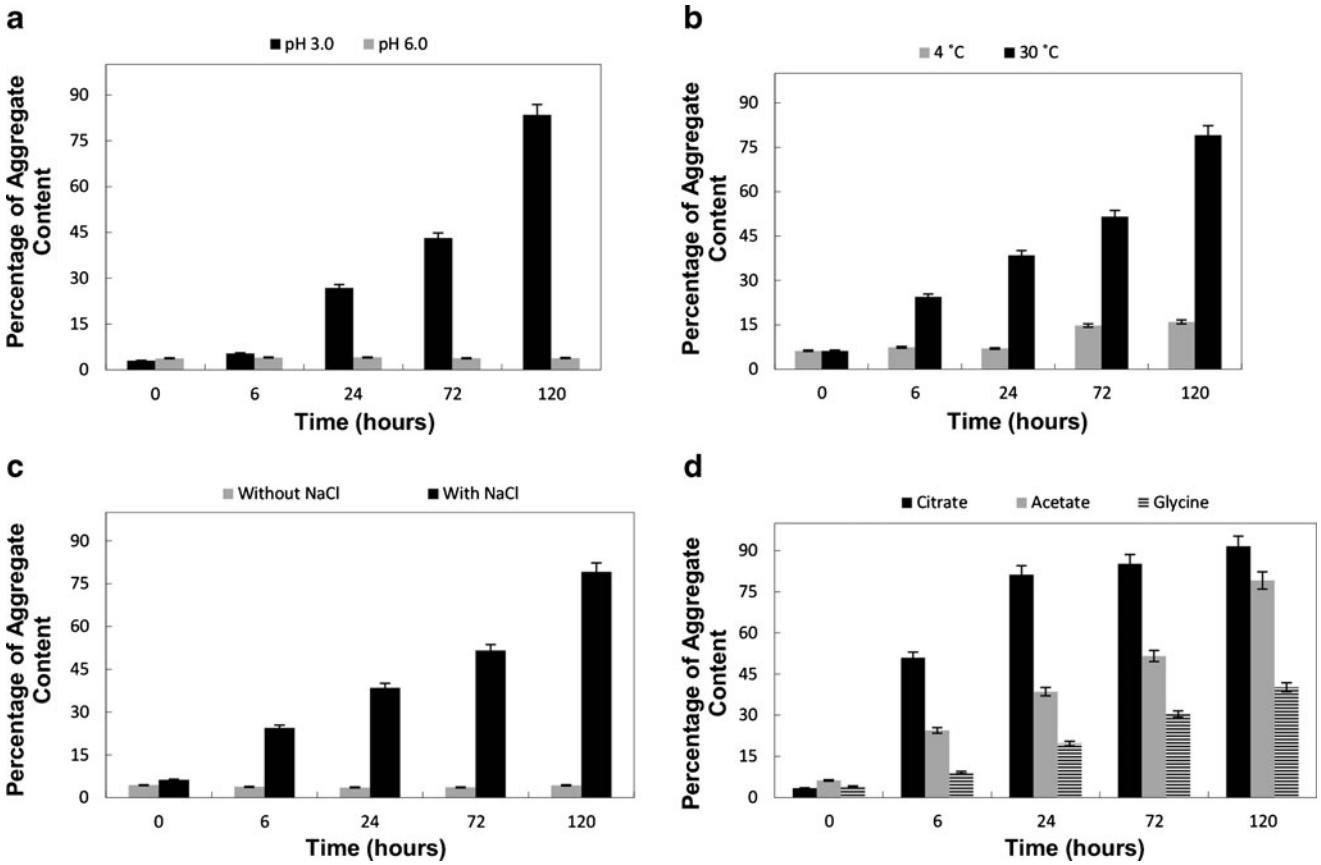


**Fig. 3.** Aggregation of a monoclonal antibody therapeutic. **a** Effect of pH (3.0 and 6.0). Operating conditions: citrate, 30°C; **b** effect of temperature (4 and 30°C). Operating conditions: acetate, 100 mM NaCl, pH 3.0; **c** effect of salt (0 and 100 mM NaCl). Operating conditions: acetate, pH 3.0, 30°C; and **d** effect of buffer (citrate, acetate, glycine). Operating conditions: 100 mM NaCl, pH 3.0, 30°C. Product concentration was 10 mg/ml in all cases. All experiments were performed in triplicate and the *error bars* show the difference between the raw data and the average

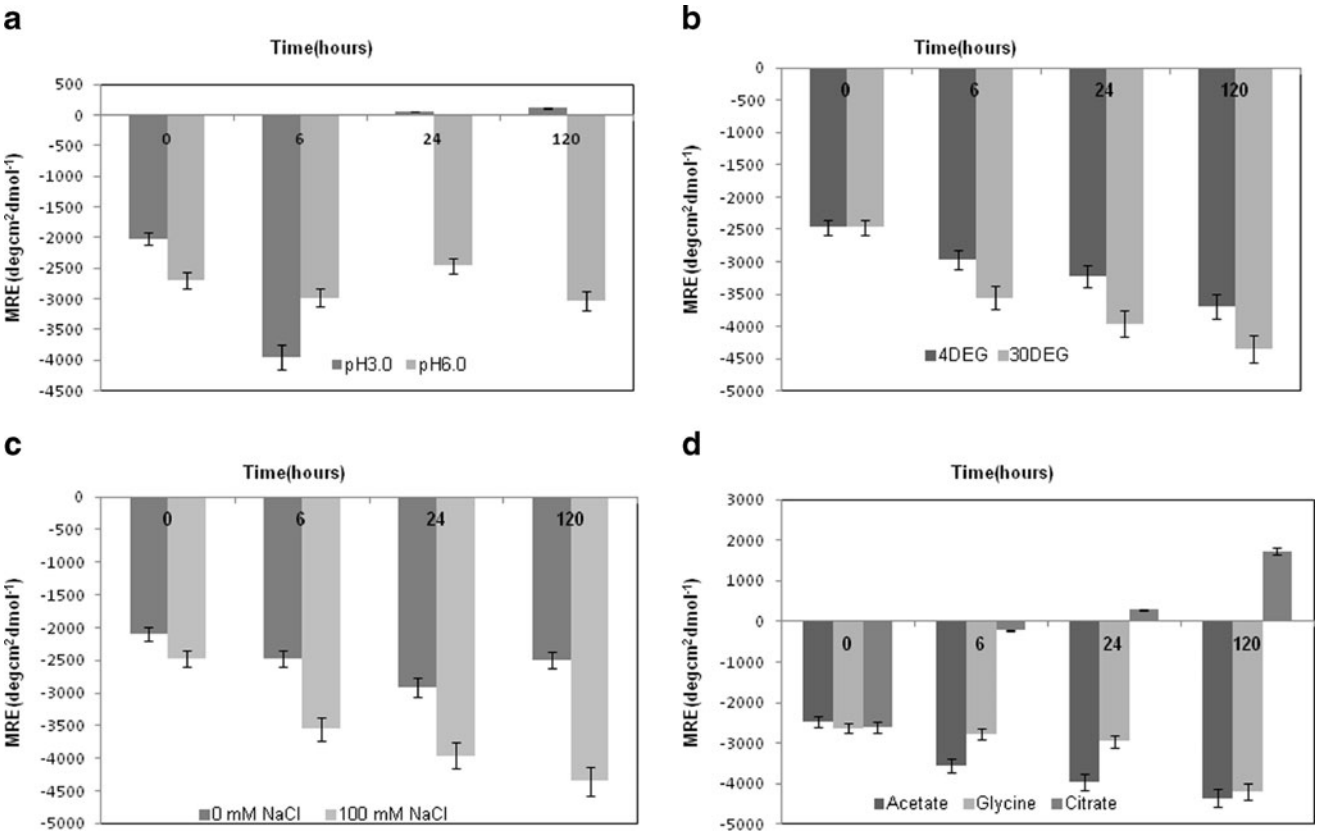


**Fig. 4.** Changes in CD MRE values at 218 nm (Far-UV) under different storage conditions. Effect of pH: **a** pH 6.0 and pH 3.0. Operating conditions: citrate, 30°C. Effect of temperature: **b** 4°C and 30°C. Operating conditions: acetate, 100 mM NaCl, pH 3.0. Effect of salt concentration: **c** 0 mM NaCl and 100 mM NaCl. Operating conditions: acetate, 30°C, pH 3.0. Effect of buffer: **d** acetate, glycine and citrate. Operating conditions: 100 mM NaCl, 30°C, pH 3.0. Product concentration was 10 mg/ml in all cases

**Table III.** Oligomer Distribution and Values of LENP Model Parameters Observed After 120 h of Incubation Under Different Storage Conditions. Values of $\tau_n$ and $\tau_g$ for All the Samples Have Been Normalized by Dividing with the Respective Values for Citrate with 100 mM NaCl at 30°C and pH 3.0. Product Concentration Was 10 mg/ml in All Cases. (M—Monomer, D—Dimer, T—Trimer, Tet—Tetramer, P—Pentamer)

| Sample | Salt concentration | Temperature | M | D | T | Tet | P | *n** | $\tau_n$ (h) | Normalized $\tau_n$[a] | $\tau_g$ (h) | Normalized $\tau_g$[b] | $\tau_n/\tau_g$ | $R^2$ | | | | |
|---|---|---|---|---|---|---|---|---|---|---|---|---|---|---|---|---|---|---|
| | | | | | | | | | | | | | | M | D | T | Tet | P |
| Citrate pH 3.0 | 0 mM NaCl | 4°C | ✓ | ✓ | ✗ | ✗ | ✗ | 2 | 4327 | 352 | 4706 | 371 | 0.9194 | 0.86 | 0.51 | – | – | – |
| | | 15°C | ✓ | ✓ | ✓ | ✗ | ✗ | 3 | 1470 | 119 | 85 | 7 | 17.2941 | 0.60 | 0.85 | 0.64 | – | – |
| | | 30°C | ✓ | ✓ | ✓ | ✓ | ✗ | 4 | 96 | 8 | 340 | 27 | 0.2823 | 0.95 | 0.82 | ND[c] | ND[c] | – |
| Citrate pH 3.0 | 50 mM NaCl | 4°C | ✓ | ✓ | ✗ | ✗ | ✗ | 2 | 2731 | 222 | 2777 | 219 | 0.9834 | 0.60 | 0.76 | – | – | – |
| | | 15°C | ✓ | ✓ | ✓ | ✗ | ✗ | 3 | 356 | 29 | 46 | 4 | 7.7391 | 0.80 | 0.64 | 0.91 | – | – |
| | | 30°C | ✓ | ✓ | ✓ | ✓ | ✗ | 4 | 26 | 2 | 13 | 1 | 2 | 0.99 | 0.60 | 0.73 | 0.97 | – |
| Citrate pH 3.0 | 100 mM NaCl | 4°C | ✓ | ✓ | ✗ | ✗ | ✗ | 2 | 280 | 23 | 302 | 24 | 0.9271 | 0.97 | 0.96 | – | – | – |
| | | 15°C | ✓ | ✓ | ✓ | ✓ | ✗ | 4 | 99 | 8 | 48 | 4 | 2.0625 | 0.98 | 0.83 | 0.87 | ND[c] | – |
| | | 30°C | ✓ | ✓ | ✓ | ✗ | ✓ | **5** | **12** | **1** | **13** | **1** | 0.9230 | 0.98 | 0.60 | ND[c] | – | ND[c] |
| Acetate pH 3.0 | 100 mM NaCl | 4°C | ✓ | ✓ | ✗ | ✗ | ✗ | 2 | 3968 | 323 | 4085 | 322 | 0.9713 | 0.92 | 0.92 | – | – | – |
| | | 15°C | ✓ | ✓ | ✗ | ✗ | ✗ | 2 | 3387 | 276 | 3912 | 308 | 0.8657 | 0.85 | 0.86 | – | – | – |
| | | 30°C | ✓ | ✓ | ✓ | ✗ | ✓ | 5 | 97 | 8 | 244 | 19 | 0.3975 | 0.89 | 0.96 | 0.97 | – | ND[c] |
| Glycine pH 3.0 | 100 mM NaCl | 30°C | ✓ | ✓ | ✓ | ✗ | ✗ | 3 | 365 | 30 | 92 | 7 | 3.9673 | 0.95 | 0.84 | ND[c] | – | – |

[a] $\tau_n$ was normalized by the value of $\tau_n$ for citrate with 100 mM NaCl at 30°C and pH 3.0 (12)
[b] $\tau_g$ was normalized by the value of $\tau_g$ for citrate with 100 mM NaCl at 30°C and pH 3.0 (13)
[c] ND—not determined (samples that had total aggregate content is <20% after 120 h)

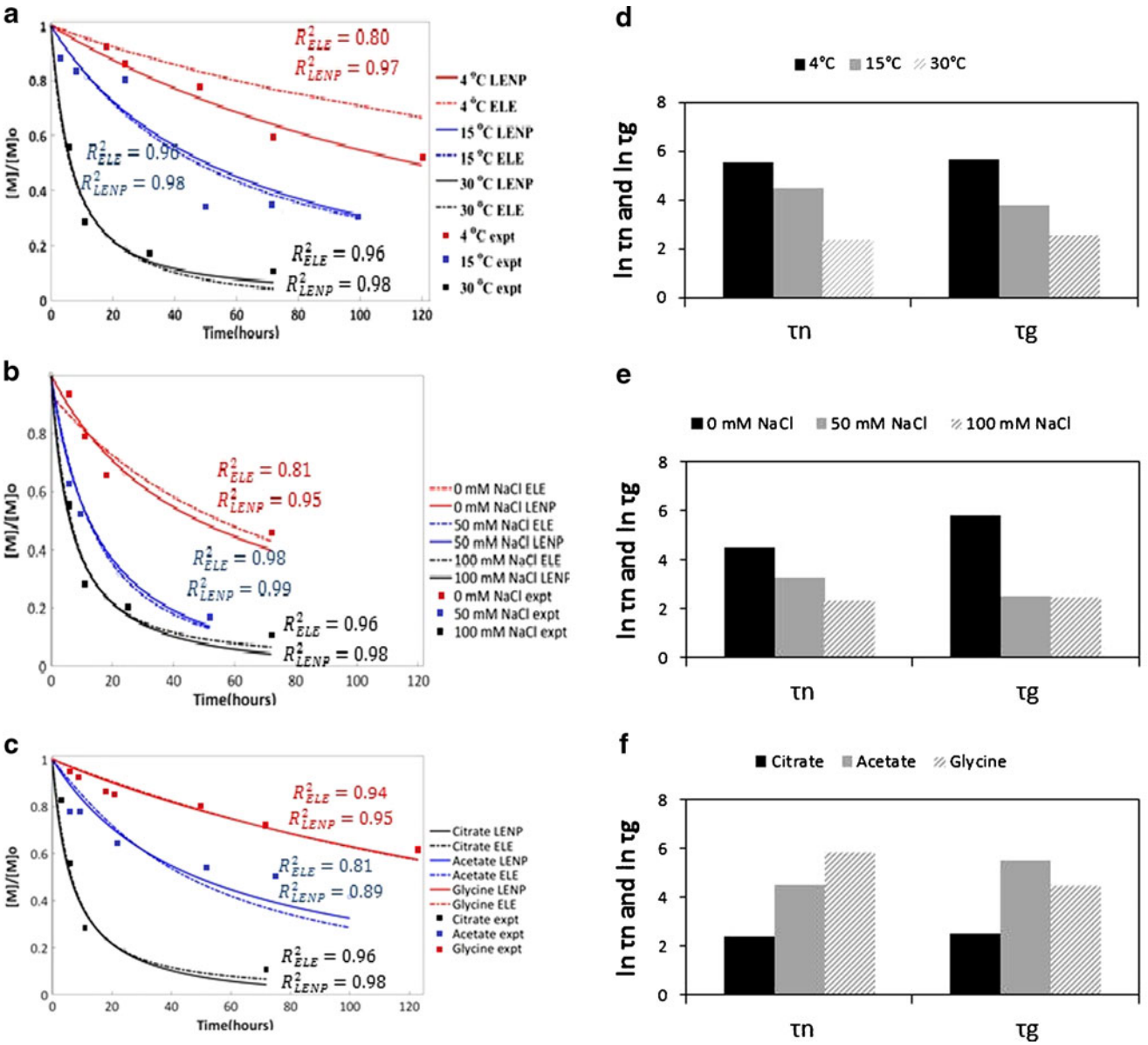


**Fig. 5.** Kinetic modeling of mAb aggregation. **a** Effect of temperature (4, 15, and 30°C), operating conditions: citrate, 100 mM NaCl, pH 3.0; **b** effect of salt concentration (0, 50, 100 mM), operating conditions: citrate, pH 3.0, 30°C; **c** effect of buffer (citrate, acetate, and glycine), operating conditions: 100 mM NaCl, pH 3.0, 30°C. **d–f** Natural log values of characteristic time scales obtained from LENP model; **d** has same conditions as **a**, **e** has same conditions as **b**, and **f** has same conditions as **c**. Product concentration was 10 mg/ml in all cases

aggregation, followed by temperature, salt concentration, and buffer species (23).

## Oligomer Distribution

Since aggregation was seen primarily in pH 3.0 buffers, these three buffers (citrate, acetate, and glycine) were further examined *via* kinetic modeling. Since the citrate buffer is the only buffer where moderate aggregation is observed in absence of salt at 4°C, aggregation was examined without salt, with 50 mM NaCl and with 100 mM NaCl. Table III presents the distribution of oligomers after 120 h of incubation in the given conditions. It is seen that all samples at 4°C have dimer as the highest order oligomer and hence this can be regarded as the critical nucleus for aggregation in this system. The limiting step for LENP is the rearrangement step (step III). In general, it is seen that as temperature increases, higher order oligomers are formed. Pentamer was the highest oligomer formed at 30°C after incubation for 120 h. Glycine offers maximum product stability at pH 3.0, and even at 30°C, trimers are observed only at later time durations.

## Kinetic Modeling

Experimental data were fitted using all the three models and rate constants at each step were obtained. The accuracy of the models was examined in each case by using the calculated constants and comparing the predicted values with the actual experimental data. In case of the F-W model, the error between the predicted and actual values of aggregate

**Table IV.** Values of ELE Model Parameters Observed After 120 h of Incubation Under Different Storage Conditions. Product Concentration Was 10 mg/ml in All Cases. (M—Monomer, D—Dimer, T—Trimer, Tet—Tetramer, P—Pentamer). ($K_1$—M × M, $K_2$—M × D, $K_3$—M × T, $K_4$—D × D, $K_{14}$—M × Tet, $K_{23}$—D × T)

| | | | | | | | | $R^2$ | | | | |
|---|---|---|---|---|---|---|---|---|---|---|---|---|
| Sample | Salt concentration | Temperature | $K_1$ | $K_2$ | $K_3$ | $K_4$ | $K_{ij}$ | M | D | T | Tet | P |
| Citrate | 0 mM NaCl | 4°C | 0.0011 | – | – | – | – | 0.58 | 0.57 | – | – | – |
| pH 3.0 | | 15°C | 0.0021 | 0.0057 | – | – | – | 0.43 | 0.72 | 0.52 | – | – |
| | | 30°C | 0.0305 | 0.0687 | – | – | – | 0.81 | 0.73 | ND[a] | ND[a] | – |
| Citrate | 50 mM NaCl | 4°C | 0.0011 | 0.2094 | – | – | – | 0.50 | 0.36 | – | – | – |
| pH 3.0 | | 15°C | 0.0099 | 0.2867 | – | – | – | 0.68 | 0.12 | 0.90 | – | – |
| | | 30°C | 0.1401 | 0.0201 | 0.4121 | 0.0661 | – | 0.98 | 0.48 | 0.28 | 0.78 | – |
| Citrate | 100 mM NaCl | 4°C | 0.0521 | 0.0741 | – | – | – | 0.80 | 0.91 | – | – | – |
| pH 3.0 | | 15°C | 0.0383 | 0.5479 | 0.0189 | 0.0791 | – | 0.96 | 0.67 | 0.84 | ND[a] | – |
| | | 30°C | 0.3069 | 0.5419 | 0.005 | – | $K_{14} = 1.4988$<br>$K_{23} = 1.848$ | 0.96 | 0.45 | ND[a] | – | ND[a] |
| Acetate | 100 mM NaCl | 4°C | 0.0019 | – | – | – | – | 0.73 | 0.75 | – | – | – |
| pH 3.0 | | 15°C | 0.0028 | – | – | – | – | 0.82 | 0.77 | – | – | – |
| | | 30°C | 0.0328 | 0.14 | 0.41 | – | $K_{14} = 0.0427$<br>$K_{23} = 1.99$ | 0.81 | 0.30 | 0.36 | – | ND[a] |
| Glycine pH 3.0 | 100 mM NaCl | 30°C | 0.0099 | 0.0614 | – | – | – | 0.94 | 0.71 | ND[a] | – | – |

[a] Not determined (samples that had total aggregate content is <20% after 120 h)

content was found to be significant (up to 60–75%) for the case of dimers and even higher for pentamer. This is likely because of the oversimplified nature of the F-W model where several actual reactions are summarized into just two pseudo-elementary steps. Further, the assumption of considering the rate of nucleation as an extremely slow step may not be justifiable as is evident from the calculated value of rate of nucleation obtained is comparable to the product of rate of growth and initial monomer concentration for case of citrate with 100 mM NaCl at 30°C and pH 3.0 ($k_1 = 9.97 \times 10^{-6}$ $s^{-1}$ and $k_2[A]_o = 8.04 \times 10^{-6}$ $s^{-1}$). Finally, accounting for the different aggregate products formed into single specie [$B$] is also a likely reason for significant errors. Thus for the application at hand, even though the F-W model has been found to be suitable for proteins like amyloid β and α-synuclein (21,22), it may not be an ideal candidate for modeling mAb aggregation.

Curve fitting was also performed with both ELE and LENP models and the kinetic parameters were estimated. Regression coefficient ($R^2$) was used to assess the quality of fits obtained with each model. It was found that for all samples, LENP gives a more precise prediction than ELE (Fig. 5a–c). The values of rate constants for ELE have been shown in Table IV. As can be seen from the Tables III and IV, the $R^2$ values for nearly all the cases are very low in the case of ELE model as compared to the LENP model. Hence, for further modeling of aggregation, LENP model was used to compute the rate of aggregation for the various HMW species. We limited the analysis to cases when the total aggregate % is <20%. Our rationale was that this is the part of spectrum which will be of interest with respect to practical applications. Our attempts to analyze cases with higher aggregate content resulted in very poor $R^2$ values, indicating a possible shift in the aggregation kinetics. This is why we

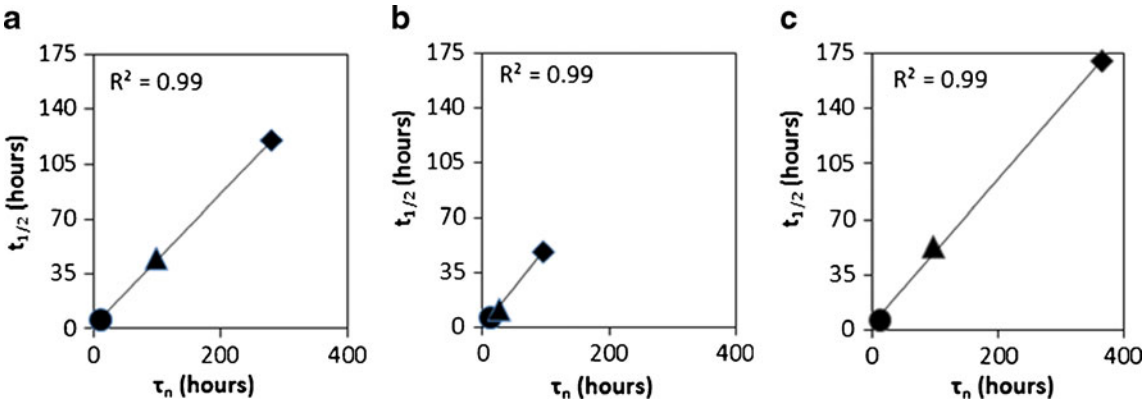


**Fig. 6.** Correlation between monomer half-life ($t_{1/2}$) and nucleation time scale ($\tau_n$). **a** Variation in temperature (4°C, *diamond*; 15°C, *triangle*; and 30°C, *circle*): Operating conditions are citrate, 100 mM NaCl, pH 3.0. **b** Variation in salt concentration (0 mM NaCl (*diamond*), 50 mM NaCl (*triangle*), and 100 mM NaCl (*circle*)): operating conditions are citrate, 30°C, pH 3.0. **c** Variation in buffer (glycine (*diamond*), acetate (*triangle*), and citrate (*circle*)): operating conditions are 100 mM NaCl, 30°C, pH 3.0. Product concentration was 10 mg/ml in all the cases

limited the scope of analysis to the cases where total aggregation is <20%.

Several key observations can be made from Table III. First, irrespective of the buffer and the salt concentration, the order of the highest order aggregate ($n^*$) increases with temperature. This is expected as the propensity of forming higher order aggregates increases at higher temperatures due to destabilization of the protein molecule. For example, in the case of citrate buffer at pH 3.0, 0 mM NaCl, there is only dimer formation at 4°C. However, at 15°C, trimer also gets formed and finally at 30°C tetramer is created.

Secondly, $R^2$ in most cases is satisfactory (>0.9). There are few cases, such as monomer formation in citrate buffer at pH 3.0, 0 mM NaCl, at 15°C when $R^2$ is quite low (0.60). However, we do not see a trend in this respect.

## DISCUSSION

As LENP model gave the most precise fits, this was utilized for further modeling and the characteristic time scales for nucleation ($\tau_n$) and growth ($\tau_g$) were compared for the different incubation conditions. Since dimers were readily observed in every sample (Table III), the stoichiometry of the nucleus ($x$) was considered to be 2 in the LENP model (27). $\delta$ was taken as 1 since trimer is also observed in samples where order of highest oligomer is greater than 2. The LENP model equations have been formulated considering that formation of new aggregates takes place via nucleation only (14).

### Effect of Temperature

An increase in temperature may result in higher protein diffusion which accelerates the probability of collision and hence the tendency of further aggregation (12). Figure 5d illustrates the change in the LENP characteristic time scales for citrate with 100 mM NaCl at pH 3.0 as temperature changes from 4 to 30°C. Both the time scales are least at 30°C implying faster nucleation and growth resulting in steeper monomer loss at a very early stage itself (Fig. 5d). Further, Fig. 6a illustrates the linear relation between nucleation time scale and experimentally observed monomer half-life when temperature is increased from 4 to 30°C. Please note that the monomer half-life has been defined as the time when 50% monomer is remaining. This suggests that monomer loss into new aggregates takes place primarily by nucleation. Similar linear correlation was observed with other citrate and acetate buffers (data not shown here).

Table III illustrates that as the temperature increases, $\tau_g$ decreases and the order of highest oligomer ($n^*$) also increases. However, there is no consistent correlation between $\tau_g$ and $n^*$. Also in the case of citrate (without salt) at pH 3.0, even though growth time scale at 15°C is smaller than at 30°C, $n^*$ is higher at 30°C.

This is likely because nucleation is so slow at 15°C that the change in the aggregated species at 15°C is only 11%, out of which trimers are only 3%. So even if higher order oligomers are formed, their concentrations are negligible.

### Effect of Salt Concentrations

Ionization from salts is known to have a destabilizing effect on the protein structure, thus resulting in an increase in the protein's susceptibility to aggregation (41). This may be attributed to hydrophobic interactions and the weakening of electrostatic interactions with increase in salt concentration. The latter results in the weakening of the repulsive forces among the positively charged protein molecules. Figure 5e illustrates the change in LENP characteristic time scales with varying salt concentration for citrate buffer at 30°C and pH 3.0. $\tau_n$ and $\tau_g$ are both estimated to be smaller for 100 mM NaCl, which explains an increase in monomer loss and formation of higher order of oligomers, respectively. The linear behavior between experimentally obtained monomer half-life and nucleation time scale is again observed as salt concentration is changed from 0 mM NaCl to 100 mM NaCl (Fig. 6b). The variation in the order of highest oligomer with salt concentration did not follow any uniform correlation with growth time scale. However, the samples with high order oligomers have small $\tau_g$ (Table III). It is widely accepted that the ratio, $\tau_n/\tau_g$, needs to be near or significantly less than 1 for one to accurately claim that nucleation dominates. Values of that ratio that are of order 10 or higher indicate that both nucleation and growth by monomer addition (*via* $\tau_g$) are important. It is seen in Table III that most (85%) of the conditions have a small ratio (<1) and can be realistically concluded as being dominated by nucleation. Cases for which the value of $\tau_n/\tau_g$ >1 are those at high temperatures (15 and 30°C). This is likely because at higher temperatures, nucleation and growth in aggregation become faster.

### Buffer Effects

The effect of different buffers on mAb aggregation is due to the complex molecular interactions that occur between buffer molecules and *Fc* domain of these antibody molecules (41). The significant effect of citrate buffer is in agreement with the Hofmeister series for anions: citrate$^{3-}$/citrate$^{2-}$>$PO4^{3-}$>$HPO_4^{2-}$>$SO_4^{2-}$ >$OAc^-$> $F^-$>$Cl^-$>$Br^-$>$I^-$>$ClO^-$ (4,40). Figure 5f presents variation in $\tau_n$ and $\tau_g$ for different buffers at 100 mM NaCl, 30°C and at pH 3.0. Citrate and glycine buffers have the least and maximum $\tau_n$, respectively, and this correlates well with the percentage level of aggregates observed in these two buffers (Tables II and III). Figure 6c suggests that as observed before, experimentally obtained monomer half-life varies linearly with the nucleation time scale when the buffer is changed. Once again, the order of highest oligomer does not follow any trend with $\tau_g$. Acetate has higher $\tau_g$ than glycine even though $n^*$ is higher for acetate (pentamer) than glycine (trimer). This means that aggregates are not formed just by addition of $\delta$ monomers, but also some condensation takes place in case of acetate.

The linear correlation between the experimentally obtained monomer half-life and nucleation time scale across variations in temperature, salt concentration, and even buffer species indicates that nucleation dominates the aggregation process in mAbs. Interestingly, the slope of all the three plots in Fig. 6 is between 0.4 and 0.5, irrespective of the storage conditions. The dominance of nucleation is probable reason why the LENP model offers the best fit (14).

## CONCLUSIONS

In this paper, aggregation behavior of monoclonal antibodies has been analyzed using kinetic analysis under commonly used processing conditions. Effect of buffer species, pH, temperature, and salt concentration has been examined on mAb aggregation. SEC and CD spectroscopy have been used to characterize the time evolution of monomer and other aggregated species. Experimental observations reveal that pH has the most significant effect on aggregation, followed by temperature, salt concentration, and buffer species. Finke-Watzky, Extended Lumry-Eyring, and Lumry-Eyring Nucleated Polymerization models have been evaluated to fit the experimental data and results have been analyzed. F-W model did not yield satisfactory fit of the data. ELE and LENP performed better with the LENP model producing the best fit. It was found that the smaller the nucleation and growth time scales, the higher is the level of aggregation. Nucleation was found to play a major role in the aggregation process and half-life was found to linearly correlate to $\tau_n$.

## REFERENCES


1. Nicolaides NC, Sass PM, Grasso L. Monoclonal antibodies: a morphing landscape for therapeutics. Drug Dev Res. 2006;67:781–9.
2. Maruyama T, Parren PWHI, Sanchez A, Rensink I, Rodriguez LL, Khan AS, *et al.* Recombinant human monoclonal antibodies to Ebola virus. J Infect Dis. 1995;179(1):S235–9.
3. Reichert JM, Rosensweig CJ, Faden LB, Dewitz MC. Monoclonal antibody successes in the clinic. Nat Biotechnol. 2005;23(9):1073–8.
4. Vázquez-Rey M, Lang DA. Aggregates in monoclonal antibody manufacturing processes. Biotechnol Bioeng. 2011;108(7):1494–508.
5. Ishikawa T, Ito T, Endo R, Nakagawa K, Sawa E, Wakamatsu K. Influence of pH on heat-induced aggregation and degradation of therapeutic monoclonal antibodies. Biol Pharm Bull. 2010;33(8):1413–7.
6. Rathore AS, Joshi V, Yadav N. Aggregation of monoclonal antibody products : formation and removal. BioPharm Int. 2013;26(3):40–5.
7. Arora I, Bansal R, Joshi V, Rathore AS. Aggregation kinetics for monoclonal antibody products. Int J Chem Eng Appl. 2014;5(5):433–8.
8. Wang W. Protein aggregation and its inhibition in biopharmaceutics. Int J Pharm. 2005;289(1):1–30.
9. Speed MA, King J, Wang DIC. Polymerization mechanism of polypeptide chain aggregation. Biotechnol Bioeng. 1997;54(4):333–43.
10. Fink AL. Protein aggregation: folding aggregates, inclusion bodies and amyloid. Fold Des. 1998;3(1):R9–23.
11. Philo JS, Arakawa T. Mechanisms of protein aggregation. Curr Pharm Biotechnol. 2009;10(4):348–51.
12. Wang W, Roberts CJ, editors. Aggregation of therapeutic proteins. New Jersey: Wiley; 2010.
13. Morris AM, Watzky MA, Finke RG. Protein aggregation kinetics, mechanism, and curve-fitting: a review of the literature. Biochim Biophys Acta. 2009;1794(3):375–97.
14. Andrews JM, Roberts CJ. A Lumry-Eyring nucleated polymerization model of protein aggregation kinetics: 1. Aggregation with pre-equilibrated unfolding. J Phys Chem B. 2007;111(27):7897–913.
15. Sanchez-Ruiz JM. Theoretical analysis of Lumry-Eyring models in differential scanning calorimetry. Biophys J. 1992;61(4):921–35.
16. Lumry R, Eyring H. Conformation changes of proteins. J Phys Chem. 1954;58(2):110–20.
17. Arosio P, Barolo G, Müller-Späth T, Wu H, Morbidelli M. Aggregation stability of a monoclonal antibody during downstream processing. Pharm Res. 2011;28(8):1884–94.
18. Nicoud L, Arosio P, Sozo M, Yates A, Norrant E, Morbidelli M. Kinetic analysis of the multistep aggregation mechanism of monoclonal antibodies. J Phys Chem B. 2014;118(36):10595–606.
19. Roberts CJ. Kinetics of irreversible protein aggregation: analysis of extended Lumry-Eyring models and implications for predicting protein shelf life. J Phys Chem B. 2003;107(5):1194–207.
20. Roberts CJ. Non-native protein aggregation kinetics. Biotechnol Bioeng. 2007;98(5):927–38.
21. Watzky MA, Morris AM, Ross ED, Finke RG. Fitting yeast and mammalian prion aggregation kinetic data with the Finke-Watzky two-step model of nucleation and autocatalytic growth. Biochemistry. 2008;47(40):10790–800.
22. Morris AM, Watzky MA, Agar JN, Finke RG. Fitting neurological protein aggregation kinetic data via a 2-step, minimal/"Ockham's razor" model: the Finke-Watzky mechanism of nucleation followed by autocatalytic surface growth. Biochemistry. 2008;47(8):2413–27.
23. Joshi V, Shivach T, Kumar V, Yadav N, Rathore A. Avoiding antibody aggregation during processing: establishing hold times. Biotechnol J. 2014;9(9):1195–205.
24. Rubinstein M, Colby RH. Polymer physics. New York: Oxford University Press; 2003.
25. Joshi V, Shivach T, Yadav N, Rathore AS. Circular dichroism spectroscopy as a tool for monitoring aggregation in monoclonal antibody therapeutics. Anal Chem. 2014;86(23):11606–13.
26. Englezos P, Kalogerakis N, editors. Applied parameter estimation for chemical engineers. New York: Marcel Dekker; 2001. 84–114 pp.
27. Brummitt RK, Nesta DP, Chang L, Kroetsch AM, Roberts J. Nonnative aggregation of an IgG1 antibody in acidic conditions, Part 2: nucleation and growth kinetics with competing growth mechanisms. J Pharm Sci. 2011;100(6):2104–19.
28. Patterson JD, Bailey BC. Solid-state physics: introduction to the theory. Springer Science & Business Media; 2007.
29. Young AT. Rayleigh scattering. Appl Opt. 1981;20(4):533–5.
30. Shukla AA, Hubbard B, Tressel T, Guhan S, Low D. Downstream processing of monoclonal antibodies—application of platform approaches. J Chromatogr B. 2007;848(1):28–39.
31. Chi EY, Krishnan S, Randolph TW, Carpenter JF. Physical stability of proteins in aqueous solution: mechanism and driving forces in nonnative protein aggregation. Pharm Res. 2003;20(9):1325–36.
32. Remmele RL, Bhat SD, Phan DH, Gombotz WR. Minimization of recombinant human Flt3 ligand aggregation at the T m plateau: a matter of thermal reversibility. Biochemistry. 1999;38(16):5241–7.
33. Azuaga AI, Dobson CM, Mateo PL, Conejero-Lara F. Unfolding and aggregation during the thermal denaturation of streptokinase. Eur J Biochem. 2002;269(16):4121–33.
34. Chen BL, Arakawa T, Hsu E, Narhi LO, Tressel TJ, Chien SL. Strategies to suppress aggregation of recombinant keratinocyte growth factor during liquid formulation development. J Pharm Sci. 1994;83(12):1657–61.
35. Chen BL, Arakawa T, Morris CF, Kenney WC, Wells CM, Pitt CG. Aggregation pathway of recombinant human keratinocyte growth factor and its stabilization. Pharm Res. 1994;11(11):1581–7.
36. Ip AY, Arakawa T, Silvers H, Ransone CM, Niven RW. Stability of recombinant consensus interferon to air-jet and ultrasonic nebulization. J Pharm Sci. 1995;84(10):1210–4.
37. Mulkerrin MG, Wetzel R. pH dependence of the reversible and irreversible thermal denaturation of gamma interferons. Biochemistry. 1989;28(16):6556–61.
38. Tsai AM, van Zanten JH, Betenbaugh II MJ. Electrostatic effect in the aggregation of heat-denatured RNase A and implications for protein additive design. Biotechnol Bioeng. 1998;59(3):281–5.
39. Tsai AM, van Zanten JH, Betenbaugh MJI. Study of protein aggregation due to heat denaturation: a structural approach using circular dichroism spectroscopy, nuclear magnetic resonance, and static light scattering. Biotechnol Bioeng. 1998;59(3):273–80.
40. Kendrick BS, Li T, Chang BS. Physical stabilization of proteins in aqueous solution. In: Carpenter JF, Manning MC, editors. Rational design of stable protein formulations—theory and practice. New York: Plenum; 2002. p. 1–19.
41. Kameoka D, Masuzaki E, Ueda T, Imoto T. Effect of buffer species on the unfolding and the aggregation of humanized IgG. J Biochem. 2007;142(3):383–91.